

Universal finite-size-scaling amplitudes of the Potts model on a torus

Hyunggyu Park* and Marcel den Nijs

Department of Physics, (FM-15), University of Washington, Seattle, Washington 98195

(Received 7 December 1987)

We derive the exact values of the universal amplitudes associated with the finite-size-scaling behavior of the free energy and interfacial free energies of the Potts model on a torus, by means of the extended-scaling method. These amplitudes vary continuously with the value of the aspect ratio of the torus. Our results make it possible to apply the type of finite-size-scaling techniques that are standard in the context of transfer-matrix calculations to Monte Carlo simulations, and thus enhance the effectiveness of these simulations in establishing the universality class of a phase transition.

I. INTRODUCTION

In this paper we derive the exact values of the universal amplitudes associated with the finite-size-scaling behavior of the free energy and interfacial free energies of the Potts model on a torus. We use the so-called extended-scaling method.^{1,2} On a torus these universal amplitudes are different from the recently obtained values on semi-infinite strips (cylinders).³⁻⁶ Our results, summarized in Tables I-IV will considerably enhance the effectiveness of Monte Carlo simulations in numerical studies of two-dimensional critical phenomena.⁷

Finite-size scaling plays an important role in numerical investigations of two-dimensional (2D) critical phenomena. The most successful applications have been for two-dimensional models on semi-infinite lattices (infinitely long cylinders) using the transfer matrix formalism.^{8,9} The interfacial free energies are defined as the difference between the free energy per unit length for different boundary conditions. For example, in the Ising model the free energy of a Bloch wall is given by the difference in free energy between a system with periodic and antiperiodic boundary conditions. The interfacial (Bloch wall) free energy η is finite in the ordered phase, vanishes in the disordered phase, and scales at criticality as

$$\eta(L) \simeq A/L, \tag{1.1}$$

with L the circumference of the cylinder. The amplitudes A are universal. They characterize the universality class of the phase transition. This is an elementary consequence of the scaling postulate.⁸ However, it was not realized until quite recently that the values of the A 's are simply related to the critical exponents; $A = 2\pi x$, with x the critical dimension of the operator conjugate to the interface imposed by the boundary condition. For example, for cyclic boundary conditions (antiperiodic boundary conditions in the Ising model) x is equal to the magnetic critical exponent $x = x_H$. The simplest derivation of these relations between universal amplitudes and critical exponents is the one using conformal invariance.³ In Sec. III we derive them by the extended-scaling method, which is more microscopic in nature. So now you simply

look for the point where η scales with L to determine the location of a critical point, and the value of A then immediately tells you to which universality class this phase transition belongs.

Our aim is to extend this type of finite-size-scaling method to Monte Carlo (MC) simulations. In MC simulations the lattice is not semi-infinite, but finite-by-finite; a torus instead of a cylinder. On the torus the interfacial free energies scale at criticality similar as on the cylinder,

$$\eta \simeq A(s)/L, \tag{1.2}$$

with $L = L_2 = sL_1$ the size of the torus, and $s = L_2/L_1$ the aspect ratio. However, the values of the amplitudes $A(s)$ are different from those on the cylinder. For example, for the Ising model we will show that the universal amplitude of the Bloch wall free energy is equal to $A(1) = \ln(1 + 2^{3/4}) = 0.9865$ at $s = 1$ (see Sec. V), instead of $A(0) = \pi/4$ at $s = 0$ (the infinite-cylinder limit). $A(s)$ varies continuously with the aspect ratio, see Fig. 1. Before we can implement our MC version of the finite-size-scaling method we must determine the exact values of these universal amplitudes $A(s)$ for each universality

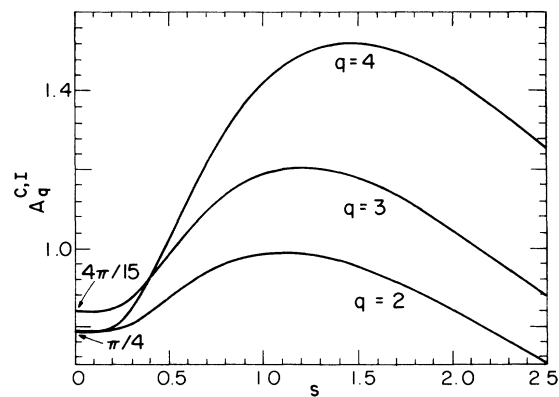


FIG. 1. The universal amplitude of the q -state Potts model, $A_q^{C,I}$, as a function of the aspect ratio s for $q = 2, 3,$ and 4 . In the $s \rightarrow 0$ limit $A_q^{C,I}$ approaches the value of the universal amplitude on a cylinder, i.e., $2\pi x_H$.

class. In this paper we derive these values for the Potts model universality class.

The disadvantage of transfer-matrix calculations is the limitation to relatively small system sizes. For example, on a typical present-day computer, the cylinder size L is bounded to less than $L \approx 12$ in systems with $q=3$ states per site or per bond. The required computer memory grows exponentially with L . Therefore, the transfer matrix method is not an adequate tool to study systems with $q > 4$, nor systems that require a large lattice to exhibit the structure of their ordered phases properly, e.g., incommensurate phases¹⁰ or commensurate phases with a large unit cell. Monte Carlo simulations are more suited for these types of problems, because simulations on large lattices are relatively easy.

Knowledge about the values of the universal finite-size-scaling amplitudes $A(s)$ is more essential in MC simulations than in transfer matrix calculations. In the transfer matrix method the free energies can be obtained numerically with machine accuracy. In MC simulations, however, configuration-averaged quantities like order parameters, specific heats, and interfacial free energies have a typical accuracy not better than 0.1%, due to statistical fluctuations. To identify the universality class of a phase transition from a finite-size-scaling analysis of, e.g., the specific heat,

$$C(L) \sim BL^{2y_T - D}, \quad (1.3)$$

you need to fit two parameters: the amplitude B , which is not universal, and the thermal critical exponent y_T which is universal (you need to subtract a regular background term as well). $D=2$ is the dimension of the system. This remains true also for interfacial free energies as long as the values of their universal amplitudes are unknown. Then Eq. (1.2) does not yield enough information to identify the universality class of the transition, and you need to perform a two-parameter fit on the first derivative of η with respect to temperature, $d\eta/dT \simeq A(s)L^{y_T-1}$, or magnetic field.

So the results of this paper enhance the effectiveness of MC simulations. MC simulations become a more accurate numerical tool to identify the universality class of a phase transition. From now on we only need to perform a one-parameter fit on the finite-size-scaling behavior of η , Eq. (1.2). Details about our MC method, such as the algorithm that we use to calculate the universal amplitudes of interfacial free energies, will be presented elsewhere, together with numerical results for the Ising and three-state Potts model. We find that this new method works very well.⁷

The outline of this paper is as follows. In Sec. II we classify all possible line defects for the Potts model on a torus that can be generated by a gauge invariant seam. All these line defects can be characterized by two permutation operators G and \tilde{G} on, respectively, the meridian and the longitudinal seam of the torus. Tables I–IV give a complete list of these line defects for $q=2, 3$, and 4.

In this paper we use the so-called extended-scaling method to determine the exact values of the universal amplitudes of the free energy of the Potts model for all these seam-type boundary conditions. In the past, ex-

tended scaling has already yielded the exact values of many of critical exponents of the Potts model.^{1,2} In this method one aims to rewrite the Potts model partition function in terms of the F -model partition function via a sequence of intermediate representations. These mappings are well established by now,^{11,12} but need to be generalized to our more general boundary conditions. We need to find the exact boundary conditions in the F model that correspond to the boundary conditions in the Potts model. The critical phase of the F model flows under renormalization to the Gaussian model.¹² Therefore, the leading finite-size-scaling behavior in the F model is identical to that in the Gaussian model with corresponding boundary conditions. In other words the F model is equivalent to a 2D Coulomb gas on a lattice, where charges that differ by a multiple of 4 are equivalent,¹ and interact at large distances in the same manner as in a conventional 2D continuum Coulomb gas. For the Potts model on a cylinder this Coulomb gas has condenser-type boundary conditions with surface charges.^{1,5}

First, in Sec. III we discuss the cylinder geometry. This serves as an introduction of the more intricate torus geometry. We give a microscopic derivation of the universal finite-size-scaling amplitudes on a cylinder. Most of them were known earlier from conformal invariance^{3–6} and some also from the extended-scaling method.⁵

In Sec. IV we obtain our general formula for the free energy of the Potts model on a torus, Eqs. (4.8) and (4.9). Our derivation is similar to the one by di Francesco, Saleur, and Zuber,¹³ who recently calculated the partition function of the Potts model [and also of the $O(n)$ model] for periodic boundary conditions. Our formula is the generalization to all types of (gauge invariant) seam-type boundary conditions.

In Sec. V we explicitly evaluate Eq. (4.9) and determine the values of the universal amplitudes for $q=2, 3$, and 4. The results are summarized in Tables II–IV at the end of this paper. We also compare our results at $q=2$ with the Onsager solution of the Ising model.¹⁴

Finally, the Appendix contains a summary of topological properties of clusters, lakes, and polygons on a torus, and our notation and sign conventions. These are essential to the discussion in Sec. IV.

II. THE q -STATE POTTS MODEL WITH INTERFACES

We consider the q -state Potts model on a torus with seam-induced interfaces. We classify such line defects by the properties of the seams. Consider the generalized q -state Potts Hamiltonian

$$H = \sum_{\langle r, r' \rangle} K \delta(\sigma_r, G_{r, r'} \sigma_{r'}). \quad (2.1)$$

The Potts spins $\sigma_r = 1, 2, \dots, q$ are defined on the sites r of a lattice \mathcal{L} , see Fig. 2. For convenience we use a square lattice, but the results of this section apply to arbitrary 2D lattices. δ is the Kronecker delta function. The $G_{r, r'}$ are the permutation operators defined on the bonds (r, r') of \mathcal{L} . $G_{r, r'}$ acts on spin $\sigma_{r'}$. It has a directional sense; $G_{r, r'} = G_{r', r}^{-1}$, i.e.,

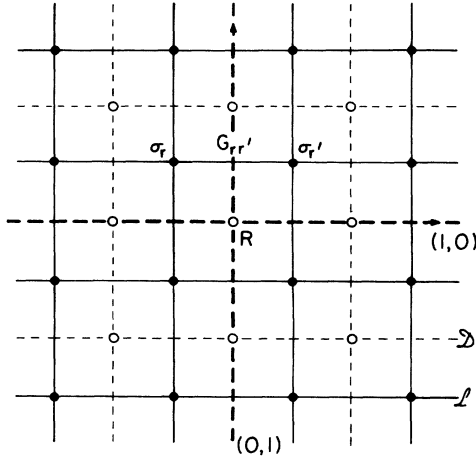


FIG. 2. The Potts-spin lattice \mathcal{L} and its dual lattice \mathcal{D} . The sites r of the Potts-spin lattice \mathcal{L} are denoted by solid circles and the sites R of the dual lattice \mathcal{D} by open circles. The operators $G_{r,r'}$ are defined on the bonds between r and r' . The dashed lines denote the $(0,1)$ and $(1,0)$ seam.

$$\delta(\sigma_r, G_{r,r'}\sigma_{r'}) = \delta(G_{r',r}\sigma_r, \sigma_{r'}) .$$

In the conventional q -state Potts model the operators G are absent; they are all equal to the identity operator $G = I$. Our purpose is to use G to induce line defects.

There are several convenient representations of the permutation operators G , for example,

$$G(3;5;6,7;1,2,4) . \quad (2.2)$$

The semicolons separate subsets of spin states. G permutes the spin states inside each subset cyclically from left to right, according to the order of these states in the string between the semicolons. In the standard terminology of group theory, the permutation operators G for the q -state Potts model form a group called the *symmetric group* of degree q and the above subsets are called *cycles*. Equation (2.2) applies to a $q = 7$ state spin model. This G does not change spin state 3 and 5, permutes the spin states $6 \leftrightarrow 7$, and permutes cyclically through the spin states $1 \rightarrow 2 \rightarrow 4 \rightarrow 1$.

We define n_i as the number of such subsets with i spin states (the number of i cycles). For the operator Eq. (2.2), these numbers are

$$\{n_1, n_2, n_3, n_4, \dots, n_7\} = \{2, 1, 1, 0, \dots, 0\} .$$

Notice that

$$\sum_{i=1}^q in_i = q . \quad (2.3)$$

An alternative representation of the permutation operators is in terms of $q \times q$ matrices, with in each row and column only one nonzero element equal to 1. For example,

$$G(2,5;1,3,4) = \begin{pmatrix} 0 & 0 & 0 & 1 & 0 \\ 0 & 0 & 0 & 0 & 1 \\ 1 & 0 & 0 & 0 & 0 \\ 0 & 0 & 1 & 0 & 0 \\ 0 & 1 & 0 & 0 & 0 \end{pmatrix} . \quad (2.4)$$

We define $z(\omega)$ as the number of spin states for which $G^\omega \sigma = \sigma$. In the matrix notation, Eq. (2.4),

$$z(\omega) = \text{Tr} G^\omega , \quad (2.5)$$

and in terms of the numbers of i -cycles n_i ,

$$z(\omega) = \sum_{i=1}^q in_i \delta(\omega, i \pmod{i}) . \quad (2.6)$$

We use the G 's to induce interfaces in the ferromagnetic-ordered phase of the Potts model. On a torus these interfaces are closed contours wrapped around the torus, so-called nonhomotopic contours. (The Appendix contains a summary of topological aspects of clusters and polygons on a torus.) We want to avoid pointlike defects. Therefore, the configuration of $G_{r,r'}$ must satisfy

$$\bigoplus_{C(0,0)} G_{r,r'} = I \quad (2.7)$$

along every homotopic contour $C(0,0)$ (closed path with zero winding numbers). The contour follows the bonds (r,r') of lattice \mathcal{L} . A configuration where the G 's around an elementary plaquette R , see Fig. 2, do not obey Eq. (2.7) contains a dislocation-type point defect located at R .

The Potts model partition function is invariant under local gauge transformations, where the q states of spin σ_r are permuted as $\sigma_r \rightarrow G'\sigma_r$, and the operators at the bonds that emerge from r are modified accordingly as $G(r,r') \rightarrow G'G(r,r')$.

Assume that Eq. (2.7) is satisfied. Then it is possible to fix the gauge in such a way that all G 's are equal to the identity operator I except along two seams. The two seams are closed loops that follow the bonds of the dual lattice \mathcal{D} , see Fig. 2; the meridian seam has winding numbers $(0,1)$ and the longitudinal seam has winding numbers $(1,0)$. After we fix the gauge the only remaining $G \neq I$ are located at bonds (r,r') that cross the two seams. According to Eq. (2.7), all the bonds that cross the seam have the same G . Moreover, the G of the meridian seam must commute with the \tilde{G} of the longitudinal seam, $[G, \tilde{G}] = 0$, to satisfy Eq. (2.7) along contours around the intersection point R of these two seams.

We associate a directional sense to each seam by placing an arrow on it, see Fig. 2. This allows us to specify the directional sense of the operator $G(r,r')$ associated with the seam. Site r (r') will always be to the left (right) of the seam with respect to the direction of the arrow on the seam. The two seams are completely characterized by their winding numbers and these arrows. Their shape and exact location are arbitrary. For example, the meridian seam in Fig. 3 moves from (a) to (b) by the gauge

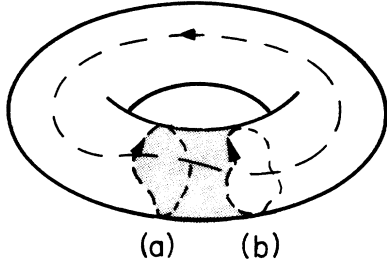


FIG. 3. Gauge invariance of seams on a torus.

transformation $G' = G^{-1}$ applied to all the sites inside the shaded area between (a) and (b).

This gauge invariance implies that all possible line defects are characterized by two commuting permutation operators G and \tilde{G} along a (0,1) and (1,0) type seam. Seams with more complicated winding numbers do not lead to new types of line defects. This confirms that all these line defects can be characterized in terms of boundary conditions. The torus becomes a flat plane with boundary conditions characterized by G and \tilde{G} , by cutting it along the two seams. Periodic (P) boundary conditions correspond to $G = I$. Cyclic (C) boundary conditions $[\sigma \rightarrow \sigma + 1 \pmod{q}]$ correspond to $G = \tilde{G}(1, 2, 3, \dots, q)$. The other types of G 's correspond to various types of twisted (T) boundary conditions. In the Ising model ($q = 2$), cyclic boundary conditions $G(1, 2)$, are identical to antiperiodic (AP) boundary conditions.

Table I lists all the possible operators G for $q = 2, 3$, and 4, and their characteristic numbers, n_i and $z(\omega)$. The commuting pairs of G and \tilde{G} for $q = 2, 3$, and 4 are listed in Tables II–IV. For $q = 2$ and $q = 3$, only $\tilde{G} = I, G$, or G^{-1} commute with G .

TABLE I. List of the permutation operators G for $q = 2, 3$, and 4. $z(\omega)$ and the number of i cycles, n_i , of G are defined in Eqs. (2.2)–(2.6). $2\pi x^G$ is the universal finite-size-scaling amplitude of the interfacial free energy induced by a boundary condition of type G on a cylinder [see Eq. (3.15)].

q	G	$\{n_1, n_2, \dots, n_q\}$	$z(\omega)$	x^G
2	I	$\{2, 0\}$	2	$\frac{1}{8}$
	C	$\{0, 1\}$	$2\delta(\omega, 2 \pmod{2})$	
3	I	$\{3, 0, 0\}$	3	$\frac{2}{15}$
	C	$\{0, 0, 1\}$	$3\delta(\omega, 3 \pmod{3})$	
	T	$\{1, 1, 0\}$	$1 + 2\delta(\omega, 2 \pmod{2})$	
4	I	$\{4, 0, 0, 0\}$	4	$\frac{1}{32}$
	C	$\{0, 0, 0, 1\}$	$4\delta(\omega, 4 \pmod{4})$	
	T_0	$\{0, 2, 0, 0\}$	$4\delta(\omega, 2 \pmod{2})$	
	T_1	$\{1, 0, 1, 0\}$	$1 + 3\delta(\omega, 3 \pmod{3})$	
	T_2	$\{2, 1, 0, 0\}$	$2 + 2\delta(\omega, 2 \pmod{2})$	

III. THE q -STATE POTTS MODEL ON A CYLINDER

We use the extended-scaling method^{1,2} to derive the finite-size-scaling properties of the Potts model on a cylinder with line defects. We use the mapping of the Potts model into the body-centered solid-on-solid (BCSOS) model^{11,1,2} and the equivalence between the critical phase of the BCSOS model and the Gaussian model¹² to derive the finite-size-scaling behavior of the free energy and the interfacial free energies. Our results are in accordance with recent results of the conformal theory.^{3–6} The extended-scaling method is microscopic in nature. Therefore, this derivation is a microscopic confirmation of the validity of the conformal ansatz for the Potts model. It is a generalization of the earlier results of Refs. 1 and 5. This section serves also as a basis for the more intricate discussion of the q -state Potts model on a torus (Sec. IV).

Consider the q -state Potts model, Eq. (2.1), on a cylinder with a line defect of type G ,

$$Z_q^G = \sum_{\{\sigma\}} \exp \left[K \sum_{\langle r, r' \rangle} \delta(\sigma_r, G_{r, r'} \sigma_{r'}) \right]. \quad (3.1)$$

We assume that Eq. (2.7) is satisfied (no pointlike defects). G is the permutation operator that remains along the seam after we fix the gauge as explained in Sec. II. G characterizes the type of line defect. The boundary conditions at the top and the bottom of the cylinder do not need to be specified, because the cylinder will be considered infinitely long. But for clarity it is useful to assume that the nearest-neighbor coupling constants inside the bottom layer and the top layer of the cylinder are infinitely strong.¹

We generalize the conventional sequence of mappings that leads to the reformulation of the Potts model as a BCSOS model,^{11,1,2} to a Potts model with line defects. The first step is to reformulate the Potts model as the random-cluster model using the high-temperature graph expansion of the Potts model¹⁵

$$\begin{aligned} Z_q^G &= \sum_{\{\sigma\}} \prod_{\langle r, r' \rangle} [1 + v \delta(\sigma_r, G_{r, r'} \sigma_{r'})] \\ &= \sum_{\text{graphs}} v^{N_b} q^{N_c} \left[\frac{n_1}{q} \right]^{N_{\text{nhc}}}. \end{aligned} \quad (3.2)$$

This is a type of bond-percolation model. The summation is over all possible graph configurations where nearest-neighbor bonds of the lattice are occupied or empty. N_b is the number of occupied bonds. Each occupied bond represents a factor $\delta(\sigma_r, G_{r, r'} \sigma_{r'})$ in the high-temperature expansion, and contributes a factor $v = \exp(K) - 1$ to the Boltzmann weight. N_c is the number of clusters in the graph. Each disconnected site also counts as a cluster. Each island-type cluster (those that do not wrap around the cylinder) contributes a factor q to the Boltzmann weight. N_{nhc} is the number of cylinder clusters (those that wrap around the cylinder, see the Appendix). Each of them contributes a factor n_1 to the Boltzmann weight. The number of unpermuted spin states n_1 of the permutation operator G , see Eqs. (2.2) and (2.5), counts how many of the q spin states obey $G\sigma = \sigma$.

The next step is to count the number of clusters in terms of the number of coastlines between clusters and lakes, i.e., in terms of polygons on the surrounding lattice \mathcal{S} ,¹¹ see Fig. 4. In a planar graph and also on a cylinder the number of polygons (coastlines) N_p is related to the number of clusters N_c , the number of bonds N_b , and the number of sites N_s , as $N_p = 2N_c - N_s + N_b$ (see Appendix). The number of nonhomotopic polygons N_{nhp} (those that wrap around the cylinder) is equal to $N_{\text{nhp}} = 2N_{\text{nhc}}$, because each cylinder cluster has two coastlines. Therefore Eq. (3.2) can be rewritten as

$$Z_q^G = q^{N_s/2} \sum_{\text{graphs}} t^{N_b} q^{N_p/2} \left(\frac{n_1}{q} \right)^{N_{\text{nhp}}/2}, \quad (3.3)$$

with $t = v/\sqrt{q}$.

Next we switch to the F model (six-vertex model) representation. Place arrows on the polygons, and count the factors \sqrt{q} and $\sqrt{n_1}$ by local phase factors. Assign a phase factor $\exp[i(\theta/4)y]$ to turns of the polygons over an angle θ . These turns take place at the sites S of the surrounding lattice \mathcal{S} . Notice that at each site S two polygons meet, and that the number of arrows pointing in and out is the same (see Fig. 4). Each polygon forms a closed loop. The arrows can be placed in two ways, clockwise or counterclockwise. Therefore the turns add up to a total angle $\pm 2\pi$ for each polygon. So the phase factors attribute a total weight \sqrt{q} to each polygon if we define y as

$$\cos \left[\frac{\pi}{2} y \right] = \frac{\sqrt{q}}{2}. \quad (3.4)$$

Ignore the boundary condition for a moment. In the arrow formulation Z_q^G is equivalent to the partition function of the six-vertex model, i.e., the trace over all possible arrow configurations on the bonds of lattice \mathcal{S} with the condition that at each vertex site S the flux of in- and out-pointing arrows is equal (see Fig. 5). At the critical

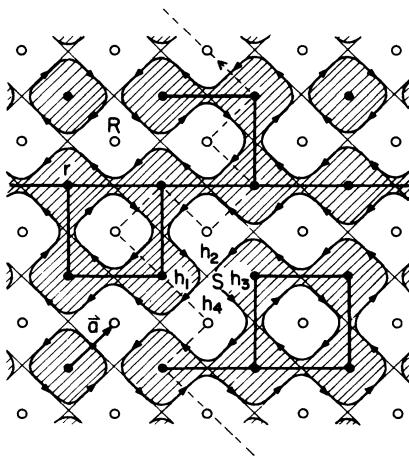


FIG. 4. Polygon representation of the random-cluster model. The polygons follows the bonds of the surrounding lattice \mathcal{S} . The shaded (unshaded) areas surrounded by polygons (coastlines) are called the clusters (lakes) in the random-cluster model formulation. The height variables h_i of the BCSOS model are defined on the faces of the surrounding lattice \mathcal{S} . The dashed line denotes a seam in the polygon representation.

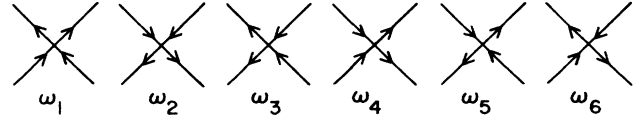


FIG. 5. Vertex states of the six-vertex model.

line of the Potts model, $t = 1$, the Boltzmann weights ω_i of this F model, are given as¹¹ $\omega_5 = \omega_6 = 1$, and $\omega_1 = \omega_2 = \omega_3 = \omega_4 = \exp(-J)$, with

$$\exp(+J) = 2 \cos \left[\frac{\pi}{4} y \right] = (2 + \sqrt{q})^{1/2}. \quad (3.5)$$

This corresponds to the exactly soluble F model.¹⁶ Varying J corresponds to moving along the critical line of the q -state Potts model in the direction of q . We restrict ourselves to $t = 1$, because we need to determine the finite-size-scaling properties at criticality only.

The local phase factors introduced above count a factor \sqrt{q} for each homotopic polygon, but add up to $1 + 1 = 2$ for nonhomotopic polygons. Each nonhomotopic polygon must have a weight $\sqrt{n_1}$. Therefore, we will associate a phase factor to the polygons each time they cross the seam. Strictly speaking this seam in the F model is different from the one in the Potts model. In the Potts model representation the bonds of the lattice \mathcal{D} dual to the Potts-spin lattice \mathcal{L} . The seam in the polygon representation follows the bonds of the lattice dual to the surrounding lattice \mathcal{S} (the dashed line in Fig. 4).

In Sec. II we introduced an orientational sense to the seams by placing an arrow on them. Such an arrow allows us to distinguish locally between the areas that are globally to the left and to the right of the seam in the F model. This is important because the shape of the seam is arbitrary. It can bend backwards. Associate to each polygon an extra weight ω (ω^{-1}) each time it crosses the seam with its arrow pointing from the left to the right (from the right to the left), with $\omega = \exp[i(\pi/2)\alpha]$.

These phase factors do not contribute to the weights of homotopic polygons, because homotopic polygons cross the seam an equal number of times in both directions. Nonhomotopic polygons pick up one of these phase factors, because they cross the seam one more time in one of the two directions. So the nonhomotopic polygons obtain a weight $\sqrt{n_1}$ if we define α as

$$\cos \left[\frac{\pi}{2} \alpha \right] = \frac{\sqrt{n_1}}{2}. \quad (3.6)$$

Recall (see Table I) that for periodic boundary conditions $n_1 = q$, and, therefore, that $\alpha = y$. For cyclic boundary conditions $n_1 = 0$ and $\alpha = 1$. For twisted boundary conditions $n_1 = 1, 2, \dots, q - 2$ and $\alpha = \frac{2}{3}, \frac{1}{2}, \frac{1}{3}, 0, \dots$.

Thus far we obtained that the partition function of the Potts model on a cylinder with a line defect of type G is proportional to the partition of the F model with a line defect of type α ;

$$Z_q^G \propto Z_F(J, \alpha), \quad (3.7)$$

with J given in Eq. (3.5) and α given in Eq. (3.6). The α sign used here and later in this paper indicates that we drop some bulk contributions (that scale as N_s), but keep all finite-size-scaling contributions.

The F model is equivalent to the so-called body-centered solid-on-solid (BCSOS) model which describes the roughening transition of crystal surfaces.¹⁷ Introduce height variables h_r on the faces of the F -model lattice \mathcal{S} . This lattice has a two-sublattice structure: the sites of the original Potts-spin lattice \mathcal{L} form one sublattice and the sites of its dual lattice \mathcal{D} the other sublattice (see Fig. 4). The heights h_r on sublattice \mathcal{L} have integer values and the heights h_r on sublattice \mathcal{D} have half-integer values. Each arrow configuration in the F model maps into a height configuration in the BCSOS model as follows. Look along a bond in the direction of the arrow. Then the height on the left is lower by $\frac{1}{2}$ than the height on the right. Notice that the height between two nearest-neighbor sites r and r' must differ by $\pm\frac{1}{2}$.

This maps Eq. (3.7) into the BCSOS Hamiltonian

$$H_{\text{BCSOS}}^G = - \sum_S J [(h_1 - h_3)^2 + (h_2 - h_4)^2] - i\pi\alpha(h_t - h_b). \quad (3.8)$$

The first summation is over all sites S of lattice \mathcal{S} , and $h_1, h_2, h_3,$ and h_4 are the four heights surrounding each site S , see Fig. 4. The line defect G in the Potts model becomes an imaginary interaction $i\pi\alpha(h_t - h_b)$. The seam in the F model runs along the bonds of the BCSOS lattice (the dual of \mathcal{S}). Label the column heights along the seam as h_i , with $i=1,2,3,\dots$. Let h_t (h_b) be the column height at the top (bottom) of the cylinder at the seam. The weight $\omega = \exp[i(\pi/2)\alpha]$ associated with each polygon crossing of the seam becomes

$$\exp[-i(\pi/2)\alpha 2(h_{i+1} - h_i)]$$

when rewritten in terms of the height differences. Added together they give $\exp[-i\pi\alpha(h_t - h_b)]$. So the critical

$$\langle \exp[-i\pi\alpha(h_t - h_b)] \rangle_{H_{\text{BCSOS}}^0} \simeq \langle \exp[-i\pi\alpha(\phi_t - \phi_b)] \rangle_{H_g} = \exp \left[-\frac{\pi^2}{2} \alpha^2 \frac{L_1}{L_2 K_g} \right], \quad (3.12)$$

where L_1 and L_2 are the height and circumference of the cylinder.

In the 2D Coulomb-gas formulation of the BCSOS model,^{1,2} the $i\pi\alpha h_t$ and $-i\pi\alpha h_b$ operator represent boundary charges $\pi\alpha$ and $-\pi\alpha$ at the top and bottom of the cylinder.^{1,5} If we assume that the Potts model coupling constant K is infinite in the top and bottom layer of the cylinder, then the top and bottom layer are equal-potential planes, and the exponent in Eq. (3.12) is simply the energy of two condenser plates at distance L_1 with surface charge densities $\pi\alpha/L_2$ and $-\pi\alpha/L_2$.

The final result is that the finite-size-scaling part of the partition function of the critical Potts model behaves as

Potts model on a cylinder is equivalent to a BCSOS model on a cylinder with periodic boundary conditions, but with boundary charges $\pm\pi\alpha$ at the top and the bottom of the cylinder,^{1,5}

$$Z_q^G \propto Z_{\text{BCSOS}}^\alpha(J) = Z_{\text{BCSOS}}^0 \langle \exp[-i\pi\alpha(h_t - h_b)] \rangle_{H_{\text{BCSOS}}^0}, \quad (3.9)$$

where the superscript 0 denotes a BCSOS model without boundary charges ($\alpha=0$). So Eq. (3.1) has now been reformulated in terms of a correlation function in the BCSOS model.

In the high-temperature phase of the BCSOS model (the critical line of the Potts model for $q \leq 4$) the discreteness of the column heights is irrelevant. To obtain the scaling-limit behavior we may relax the constraint that the height variables h_r are (half) integers and replace them by Gaussian variables ϕ_r which take real values. See Ref. 12 for details of this renormalization procedure from the BCSOS model to the Gaussian model. So the scaling-limit behavior of the BCSOS model is equivalent to that of the Gaussian model

$$Z_g = \sum_{\{\phi_r\}} \exp \left[-\frac{K_g}{2} \sum_r [(\phi_{r+\hat{e}_1} - \phi_r)^2 + (\phi_{r+\hat{e}_2} - \phi_r)^2] \right]. \quad (3.10)$$

The value of the Gaussian coupling constant K_g follows from the Baxter solution of the eight-vertex model¹⁸ or the Lieb solution of the F model,¹⁶

$$K_g = \pi x = \pi(2 - y), \quad (3.11)$$

with y defined in Eq. (3.4).

This identification allows us to calculate the scaling-limit behavior of BCSOS model correlation functions, such as Eq. (3.9):

$$Z_q^G \propto Z_g(K_g) \exp \left[-\frac{\pi^2}{2} \alpha^2 \frac{L_1}{L_2 K_g} \right]. \quad (3.13)$$

The interfacial free energies η^G associated with the operator G (see Table I) is defined as

$$\eta^G = \lim_{L_1 \rightarrow \infty} \frac{1}{L_1} \ln \frac{Z_q^P}{Z_q^G}, \quad (3.14)$$

where Z_q^P is the partition function with periodic boundary conditions; $\alpha=q$. The universal amplitudes A^G of the interfacial free energies η^G behave according to Eq. (3.13) as

$$A^G = \lim_{L_2 \rightarrow \infty} L_2 \eta^G = 2\pi \frac{(\alpha^2 - y^2)}{4x} \equiv 2\pi x^G. \quad (3.15)$$

The explicit values of x^G for the different boundary conditions are listed in Table I. They are the critical dimensions of Potts model operators associated with the interfaces characterized by G . For example, the magnetic operator of the Potts model is associated with the cyclic boundary condition. The extended-scaling relation for the magnetic critical exponent x_H was obtained in Ref. 1 via the same set of mappings from the scaling behavior of the spin-spin correlation function. Indeed Eq. (3.15) gives the extended-scaling relation for x_H when $\alpha=1$ (see also, Ref. 4, where the values of x^G listed in Table I are derived from the conformal theory).

From Eq. (3.13) it follows that the free energy per unit volume scales as

$$\begin{aligned} f_q^G &= -\frac{1}{L_1 L_2} \ln Z_q^G \\ &= f_{\text{bulk}} - \frac{\pi}{6} \left[1 - \frac{3\alpha^2}{x} \right] \frac{1}{L_2^2} + \dots \end{aligned} \quad (3.16)$$

The factor $\pi/6$ is the finite-size-scaling contribution of the Gaussian model with periodic boundary conditions (no boundary charges on an infinitely long cylinder). For a Potts model with periodic boundary conditions, Eq. (3.16) simplifies to

$$\begin{aligned} f_q^P &= f_{\text{bulk}} - \frac{\pi}{6} \left[1 - \frac{3y^2}{x} \right] \frac{1}{L_2^2} + \dots \\ &= f_{\text{bulk}} - \frac{\pi}{6} c \frac{1}{L_2^2} + \dots, \end{aligned} \quad (3.17)$$

with $c = 1 - 3y^2/x$ the definition of the central charge of the conformal theory.⁵

IV. THE POTTS MODEL ON A TORUS

We derive the universal finite-size-scaling amplitudes for the Potts model on a torus. The discussion is similar, but more intricate than for the Potts model on a cylinder in Sec. III. On a cylinder the clusters and lakes that wrap around the cylinder can only have winding numbers (1,0). On a torus many more types of clusters and lakes are possible. We distinguish between islands, ponds, cylinder clusters (CC's), cylinder lakes (CL's), torus clusters (TC's), and torus lakes (TL's) (see Fig. 6). These types of clusters and lakes are distinguished by the winding numbers (ω_1, ω_2) of the contours that you can draw on them. In our notation, contours and polygons are closed non-self-intersecting loops, while loops and walks are allowed to self-intersect.

On island-type clusters [Fig. 6(a)] and pond-type lakes [Fig. 6(c)] it is possible to draw only (0,0) type contours. On cylinder clusters and cylinder lakes [Fig. 6(b)], it is possible to draw only one type of contour with nonzero winding numbers (ω_1, ω_2) . On a torus cluster [Fig. 6(c)], and a torus lake [Fig. 6(a)], it is possible to draw two independent contours with winding numbers (0,1) and (1,0). Topological aspects play an important role in this section. For clarity, the topological properties of clusters

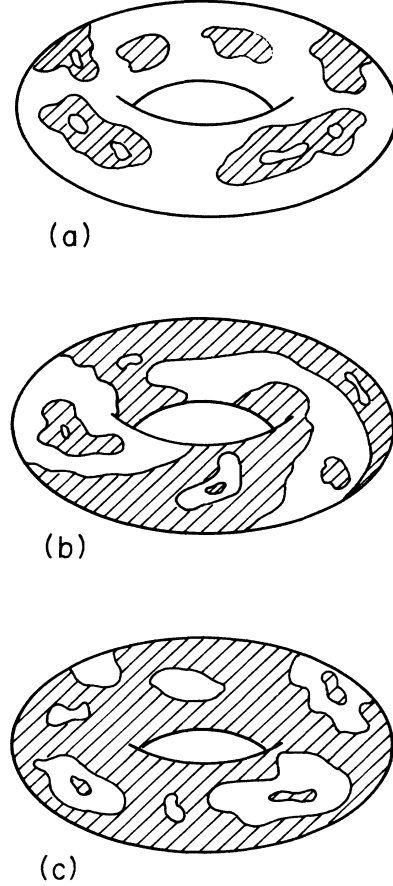


FIG. 6. Clusters and lakes on a torus. (a) A configuration with one torus lake (only islands); (b) a configuration with one cylinder cluster and one cylinder lake with winding numbers (1,2); (c) a configuration with one torus cluster (only ponds).

and contours on a torus are summarized in the Appendix, together with our notation and sign conventions.

Consider the q -state Potts model, Eq. (3.1), on a torus with permutation operators $G(r, r')$ along the meridian seam (0,1) and $\bar{G}(r, r')$ along the longitudinal seam (1,0). G and \bar{G} commute, $[G, \bar{G}] = 0$. They characterize all possible seam-induced line-defect structures (see Sec. II and Tables II–IV).

The random-cluster model formulation of the Potts model on a torus is more complicated than on a cylinder because the various types of clusters have different weights. Consider the trace over the spin states in Eq. (3.2). The weight of a cluster is equal to the number of spin states σ for which $(\prod G)\sigma = \sigma$ is satisfied simultaneously along every possible closed walk across the cluster. The product is over all G operators that you encounter along the path. Along (0,0) walks the product is equal to the identity operator [see Eq. (2.7)]. Therefore, island-type clusters have again a weight q . On a cylinder cluster (CC) with winding numbers (ω_1, ω_2) all walks are superpositions of (0,0) and (ω_1, ω_2) type contours. Therefore, cylinder clusters have a weight

$$C(G, \bar{G}; \omega_1, \omega_2) = \text{Tr}(G^{\omega_1} \bar{G}^{\omega_2}),$$

which is the number of spin states that satisfy $G^{\omega_1} \tilde{G}^{\omega_2} \sigma = \sigma$. On a torus cluster (TC) all walks are superpositions of the (0,0), (0,1), and (1,0) type contours. Therefore, torus clusters have a weight $T(G, \tilde{G})$, equal to the number of spin states that satisfy simultaneously $G\sigma = \sigma$ and $\tilde{G}\sigma = \sigma$.

The combinations $\tilde{G} = I, G$, and G^{-1} play a special role. They represent the complete set of line defects for $q = 2$ and 3 (see Tables II–IV). For these combinations the cluster weights C and T are easily expressed in terms of the characteristic parameters $z(\omega)$ and n_1 defined in Eqs. (2.2)–(2.6).

$$\begin{aligned} C(G, I; \omega_1, \omega_2) &= z(\omega_1), \\ C(I, G; \omega_1, \omega_2) &= z(\omega_2), \\ C(G, G; \omega_1, \omega_2) &= z(\omega_1 + \omega_2), \\ C(G, G^{-1}; \omega_1, \omega_2) &= z(\omega_1 - \omega_2), \end{aligned} \quad (4.1)$$

and

$$T(G, I) = T(I, G) = T(G, G) = T(G, G^{-1}) = z(1) = n_1. \quad (4.2)$$

Thus, in the random cluster model formulation the partition function of the Potts model on a torus reads

$$\begin{aligned} Z_q^{G\tilde{G}} &= \sum_{\{\text{CC's}\}} v^{N_b} q^{N_c} \left[\frac{C(G, \tilde{G}; \omega_1, \omega_2)}{q} \right]^{N_{\text{nhc}}} \\ &+ \sum_{\{\text{TC's}\}} v^{N_b} q^{N_c - 1} T(G, \tilde{G}) + \sum_{\{\text{TL's}\}} v^{N_b} q^{N_c}. \end{aligned} \quad (4.3)$$

Compare this with Eq. (3.2). N_{nhc} is the number of cylinder clusters. All the cylinder clusters (and cylinder lakes) in a configuration have the same winding numbers (see the Appendix). In Eq. (4.3) the configurations are divided into three types. The first summation is over all configurations with cylinder clusters, the second over all

configurations with one torus cluster, the third over all configurations with one torus lake (all clusters are islands). This separation is possible because a configuration must contain one torus cluster, or one torus lake, or (an equal number of) cylinder clusters and cylinder lakes. These three types of clusters and lakes cannot coexist together, and a configuration can contain at most one torus cluster or one torus lake (see the Appendix).

Next, we need to reformulate this in terms of polygon configurations on the surrounding lattice \mathcal{S} . The polygons are the coastlines between clusters and lakes. It is convenient to think of the clusters as continuum-type objects (see Fig. 6) but in reality the clusters have a lattice structure. Each site r of lattice \mathcal{L} is part of a cluster, and each site R of lattice \mathcal{D} is part of a lake (see Fig. 4). The Euler relation states that in any configuration $N_c = N_s - N_b + N_l$, with N_s the number of sites in lattice \mathcal{L} , and N_l the number of independent nonhomotopic contours on the clusters (see the Appendix).

In configurations with only island-type clusters [the third term in Eq. (4.3)] [see Fig. 6(a)], N_l is equal to the number of ponds inside the clusters (the torus lake does not count). The number of coastlines N_p is equal to $N_p = N_c + N_l$ (see the Appendix). In configurations with cylinder clusters [the first term in Eq. (4.3)] [see Fig. 6(b)], N_l is equal to the number of ponds plus the number of cylinder clusters. The number of nonhomotopic coastlines N_{nhp} (those that wrap around the torus) is equal to $N_{\text{nhp}} = 2N_{\text{nhc}}$ (each cylinder cluster has two nonhomotopic coastlines). The total number of coast lines N_p is again equal to $N_p = N_c + N_l$. In configurations with one torus cluster [the second term in Eq. (4.3)] [see Fig. 6(c)], N_l is equal to the number of ponds minus 1 (all lakes are ponds) plus 2 (the torus cluster counts twice). So the number of coast lines N_p is equal to $N_p = N_c + N_l - 2$ (see the Appendix).

Thus, in the polygon representation the partition function of the Potts model on a torus reads

$$Z_q^{G\tilde{G}} = q^{N_s/2} \left[\sum_{\{\text{CC's}\}} t^{N_b} q^{N_p/2} \left[\frac{C(G, \tilde{G}; \omega_1, \omega_2)}{q} \right]^{N_{\text{nhc}}/2} + \sum_{\{\text{TC's}\}} t^{N_b} q^{N_p/2} T(G, \tilde{G}) + \sum_{\{\text{TL's}\}} t^{N_b} q^{N_p/2} \right]. \quad (4.4)$$

The temperature parameter, $t = v/\sqrt{q}$, represents a difference in energy per unit area between clusters and lakes. This energy difference vanishes along the critical line of the Potts model. $t = 1$ is the critical line when \mathcal{L} is a self-dual lattice (the square lattice). At criticality we can complete the switch from cluster configurations to polygon (coast line) configurations, because the Boltzmann weight becomes fully determined by the number of coast lines of each type.

The second and third summations in (4.4) correspond to the summation over all configurations with only homotopic polygons. The set of configurations with one torus cluster (only ponds) is dual to the set with one torus lake (only islands) under reversal of the cluster-lake labels (see the Appendix). So each homotopic polygon configuration gives rise to one of the torus-cluster

configurations in the Potts model on lattice \mathcal{L} and one of the torus-lake configurations in the dual Potts model on the dual lattice \mathcal{D} .

The first summation in Eq. (4.4) corresponds to the summation over all possible configurations with an even (nonzero) number of nonhomotopic polygons. The set of configurations with cylinder clusters is self-dual under reversal of the cluster-lake labels (see the Appendix). The number of cylinder clusters in a configuration is equal to the number of cylinder lakes. So each nonhomotopic polygon configuration gives rise to one configuration with cylinder clusters in the Potts model on lattice \mathcal{L} and one in the dual Potts model on lattice \mathcal{D} .

Thus in the case of a self-dual lattice \mathcal{L} , Eq. (4.4) simplifies at criticality, $t = 1$, as

$$Z_q^{G\tilde{G}} = q^{N_s/2} \sum_{\{N_{\text{nhp}}=\text{even}\}} q^{N_p/2} \left[\frac{C(G, \tilde{G}; \omega_1, \omega_2)}{q} \right]^{N_{\text{nhp}}/2} + \frac{1}{2} [T(G, \tilde{G}) - 1] \sum_{\{N_{\text{nhp}}=0\}} q^{N_p/2}. \quad (4.5)$$

The first summation is over all possible configurations with an even number of nonhomotopic polygons. For convenience we include the $N_{\text{nhp}}=0$ configurations, i.e., all configurations with only homotopic polygons in this summation as well, and subtract their contributions in the second summation accordingly.

Next we reformulate the Boltzmann weights of the polygons in terms of local phase factors by introducing arrows on the polygons. Again the phase factors $\exp[i(\theta/4)y]$ associated with the local turns of the polygons over an angle θ [see Eq. (3.4)], count the weights \sqrt{q} of the homotopic polygons. Again these phase factors fail to count the weights C of the nonhomotopic polygons. In analogy with Eq. (3.6) we rewrite the weights C as

$$\cos \left[\frac{\pi}{2} \alpha(G, \tilde{G}; \omega_1, \omega_2) \right] = \frac{[C(G, \tilde{G}; \omega_1, \omega_2)]^{1/2}}{2}, \quad (4.6)$$

and assign a phase factor

$$\exp[\pm i(\pi/2)\alpha(G, \tilde{G}; \omega_1, \omega_2)]$$

to each nonhomotopic polygon according to the two possible directions of its arrow. Although the final result, Eq. (4.8), does not depend on it, we need to introduce a sign convention to identify the two phase factors to the two possible arrow directions on the nonhomotopic polygons. By convention we identify the $\exp[+i(\pi/2)\alpha]$ phase factor with the arrow that points in the direction with positive ω_1 and with positive ω_2 for a (0,1) polygon. Recall that the signs of the winding numbers are defined with respect to the directions of the arrows on the meridian and longitudinal seams (see the Appendix).

In the F model the configurations are characterized by two polarizations, P_1 and P_2 . P_1 is the net polarization of the arrows along the meridian seam, and P_2 the net polarization along the longitudinal seam. P_1 and P_2 are topological numbers independent of the shape and location of these two seams (gauge invariance). P_i is $\frac{1}{2}$ times the net number of arrows that point through the seam from the left to the right with respect to the direction of the arrow on the seam. P_1 and P_2 are integers, because the number of nonhomotopic polygons N_{nhp} is even.

We need to associate these polarizations to the phase

factors (4.6). The polygons have the following topological properties (see the Appendix): (i) the winding numbers of nonhomotopic polygons are coprime, (ii) nonhomotopic polygons can coexist on a torus if and only if their winding numbers are the same, and (iii) homotopic polygons do not contribute to the polarizations. This implies that a configuration in the F model with a nonzero polarization (P_1, P_2) can contain only one type of nonhomotopic polygon with winding numbers (ω_1, ω_2) such that

$$\omega_i = \frac{P_i}{g(P_1, P_2)} \quad (i=1,2), \quad (4.7)$$

with $g(P_1, P_2)$ equal to the greatest common divisor of P_1 and P_2 . To be consistent with our sign convention $g(P_1, P_2)$ must have the same sign as P_1 . By definition $g(P_1, 0) = P_1$ and $g(0, P_2) = P_2$.

The set of configurations with $P_1 = P_2 = 0$ is special. Not only does it include all the configurations where all the polygons are homotopic, it also includes all types of configurations with nonhomotopic clusters. Consider any configuration with cylinder clusters. The number of nonhomotopic polygons (the coast lines of these cylinder clusters) is even. So it is possible to draw arrow configurations on these polygons such that $P_1 = P_2 = 0$.

Thus, in the F -model formulation each nonhomotopic polygon configuration characterized by winding numbers (ω_1, ω_2) is distributed over the configurations with polarizations (P_1, P_2) that satisfy Eq. (4.7), and also over a subset of the configurations with $P_1 = P_2 = 0$. The nonhomotopic polygons obtain the correct weights if we assign a phase factor $\exp[i\pi\alpha g(P_1, P_2)]$ to the partition function of the F model with polarization (P_1, P_2). $2g(P_1, P_2)$ is equal to the net number of arrows on the nonhomotopic polygons that point in the direction with positive ω_1 .

The second term in Eq. (4.5) can be considered as a special case of the above. There the summation is restricted to all configurations with only homotopic polygons. The nonhomotopic polygon configurations obtain a zero weight if we choose $\alpha=1$ regardless of the values of (ω_1, ω_2) [see Eq. (4.6)].

Thus in the F -model formulation the partition function of the Potts model on a torus reads,

$$Z_q^{G\tilde{G}} = q^{N_s/2} \sum_{P_1, P_2 \in \mathbb{Z}} Z_F^{P_1, P_2} \{ \cos[\pi g(P_1, P_2)\alpha(G, \tilde{G}; \omega_1, \omega_2)] + \frac{1}{2} [T(G, \tilde{G}) - 1] \cos[\pi g(P_1, P_2)] \}. \quad (4.8)$$

The summation is over all integer values of P_1 and P_2 . $Z_F^{P_1, P_2}$ is the partition function of the F model with periodic boundary conditions, with a given polarization (P_1, P_2). We used that $Z_F^{P_1, P_2} = Z_F^{-P_1, -P_2}$.

In the BCSOS model formulation of the F model (see Sec. III) the arrows represent steps in a crystal surface. The polarizations (P_1, P_2) represent boundary conditions where the surface has a fixed average tilt in both directions. The

high-temperature phase of the BCSOS model, i.e., the critical line of the Potts model for $q \leq 4$, flows under renormalization to the Gaussian model, Eqs. (3.10) and (3.11). The tilt angles are conserved under the renormalization transformation. Therefore, the leading finite-size-scaling contribution of each $Z_F^{P_1, P_2}$ is the same as in the Gaussian model, i.e.,

$$Z_q^{G\tilde{G}} \propto \sum_{P_1, P_2 \in \mathbb{Z}} Z_g^{P_1, P_2} \{ \cos[\pi g(P_1, P_2) \alpha(G, \tilde{G}; \omega_1, \omega_2)] + \frac{1}{2} [T(G, \tilde{G}) - 1] \cos[\pi g(P_1, P_2)] \}, \quad (4.9)$$

with $Z_g^{P_1, P_2}$ the partition function of the Gaussian model with the step boundary conditions: $\phi(x + L_1, y) = \phi(x, y) + P_1$ and $\phi(x, y + L_2) = \phi(x, y) + P_2$, with L_1 and L_2 the meridian and longitudinal lengths of the torus. As before the \propto sign only indicates that we drop some bulk contributions but keep all the finite-size-scaling contributions.

These Gaussian partition functions are easily evaluated:

$$\frac{Z_g^{P_1, P_2}}{Z_g^{0,0}} = \exp \left[-\frac{K_g}{2} \left[sP_1^2 + \frac{1}{s}P_2^2 \right] \right], \quad (4.10)$$

where $s = L_2/L_1$ is the aspect ratio. The finite-size-scaling part of $Z_G^{0,0}$ is proportional to¹⁹

$$Z_g^{0,0} \propto \frac{1}{\eta^2} \left[\frac{K_g}{2\pi s} \right]^{1/2}, \quad (4.11)$$

with η the Dedekind eta function²⁰

$$\eta = \exp \left[-\frac{\pi}{12} s \right] \prod_{n=1}^{\infty} \left[1 - \exp(-2\pi sn) \right]. \quad (4.12)$$

Equation (4.9) includes the earlier result of di Francesco *et al.*¹³ for periodic boundary conditions, $G = \tilde{G} = I$. Our result, Eq. (4.9), is the generalization of this to all possible seam-type boundary conditions for the Potts model on a torus. It is also interesting to compare Eq. (4.9) with the operator content of the $q=2$ and $q=3$ state Potts model as predicted from the conformal theory.⁴

V. FINITE-SIZE SCALING FOR THE q -STATE POTTS MODEL ON A TORUS

In the previous section we obtain the exact expression, Eq. (4.8), for the partition function of the q -state Potts model on a torus with general boundary conditions in the BCSOS model (F model) representation. Equation (4.9) where we replace the F -model partition functions by Gaussian model partition functions gives the leading finite-size-scaling behavior. In this section we evaluate Eq. (4.9) explicitly at $q=2, 3$, and 4 for the specific

boundary conditions listed in Table I. Moreover, we compare our results at $q=2$ with the exact solution of the Ising model on a torus.¹⁴

On a torus the universal amplitudes of the interfacial free energies are defined in a similar way as on a cylinder, Eqs. (3.14) and (3.15),

$$A_q^{G\tilde{G}} = \lim_{L_1, L_2 \rightarrow \infty} \left[\frac{L_2}{L_1} \ln \left[\frac{Z_q^P}{Z_q^{G\tilde{G}}} \right] \right] \quad (5.1)$$

at fixed aspect ratio $s = L_2/L_1$. $Z_q^P = Z_q^{I,I}$ is the partition function of the Potts model with periodic boundary conditions. $Z_q^{G\tilde{G}}$ maps into $Z_q^{G\tilde{G}}$ under a rotation of the lattice over an angle of 90° , i.e., by replacing s by $1/s$. It follows that $A_q^{G\tilde{G}}(s) = s^2 A_q^{G\tilde{G}}(1/s)$.

For later convenience we define

$$[n, m] \equiv \frac{1}{2} \sum_{\substack{P_1 \in n\mathbb{Z} \\ P_2 \in m\mathbb{Z}}} Z_g^{P_1, P_2}(K_g), \quad (5.2)$$

with n and m positive integers. $[n, m]$ can be written in terms of the Jacobi's theta functions θ_3 (Ref. 20)

$$\theta_3(z) = \sum_{n \in \mathbb{Z}} \exp(-\pi n z^2), \quad (5.3)$$

as

$$[n, m] = \frac{1}{2m\eta^2} \theta_3 \left[\frac{xn^2}{2} s \right] \theta_3 \left[\frac{2}{xm^2} s \right], \quad (5.4)$$

by using Eqs. (4.10)–(4.12), and the Jacobi's transformation formula²⁰

$$\theta_3(z) = \frac{1}{\sqrt{z}} \theta_3 \left[\frac{1}{z} \right]. \quad (5.5)$$

Notice that $[m, n]$ is equivalent to $[n, m]$ under replacement of s by $1/s$.

First consider the Ising model ($q=2$). From Eqs. (3.4) and (3.11) it follows that $y = \frac{1}{2}$ and $K_g = \pi x = \frac{3}{2}\pi$. For periodic boundary conditions it follows from Eqs. (4.1) and (4.2) that $C(I, I; \omega_1, \omega_2) = q=2$ and $T(I, I) = q=2$. So $\alpha = y = \frac{1}{2}$ [see Eqs. (3.4) and (4.6)]. Then, Eq. (4.9) can be evaluated explicitly as

$$\begin{aligned} Z_{q=2}^P &\propto \sum_{P_1, P_2 \in \mathbb{Z}} \left[\cos \left[\frac{\pi}{2} g(P_1, P_2) \right] + \frac{1}{2} \cos[\pi g(P_1, P_2)] \right] Z_G^{P_1, P_2} \\ &= \left[\frac{3}{2} \sum_{\substack{g(P_1, P_2)=0 \\ (\text{mod } 4)}} - \frac{1}{2} \sum_{\substack{g(P_1, P_2)=1, 2, 3 \\ (\text{mod } 4)}} \right] Z_G^{P_1, P_2} = \left[\frac{3}{2} \sum_{P_1, P_2 \in 4\mathbb{Z}} - \frac{1}{2} \left[\sum_{P_1, P_2 \in \mathbb{Z}} - \sum_{P_1, P_2 \in 4\mathbb{Z}} \right] \right] Z_G^{P_1, P_2} \\ &= \left[2 \sum_{P_1, P_2 \in 4\mathbb{Z}} - \frac{1}{2} \sum_{P_1, P_2 \in \mathbb{Z}} \right] Z_G^{P_1, P_2} = 4[4, 4] - [1, 1]. \end{aligned} \quad (5.6)$$

Expressed in terms of the theta functions this becomes

$$Z_{q=2}^P \propto \frac{1}{2\eta^2} \left[\theta_3 \left[\frac{s}{12} \right] \theta_3(12s) - \theta_3 \left[\frac{4s}{3} \right] \theta_3 \left[\frac{3s}{4} \right] \right]. \quad (5.7)$$

There are only three more types of boundary conditions in the Ising model on a torus. These three partition functions can be written as

$$\begin{aligned} Z_{q=2}^{C,I} &\propto Z_{q=2}^P + 2[2,1] - 4[4,2], \\ Z_{q=2}^{I,C} &\propto Z_{q=2}^P + 2[1,2] - 4[2,4], \\ Z_{q=2}^{C,C} &\propto -Z_{q=2}^P - 2[2,1] + 4[4,2] - 2[1,2] + 4[2,4]. \end{aligned} \quad (5.8)$$

$Z_{q=2}^{C,I}$ and $Z_{q=2}^{I,C}$ are the partition functions with antiperiodic boundary conditions along one of the two seams. $Z_{q=2}^{C,C}$ is the partition function with antiperiodic boundary conditions in both directions. Notice that $Z_{q=2}^P = Z_{q=2}^{I,C} + Z_{q=2}^{C,I} + Z_{q=2}^{C,C}$.

In Fig. 1 the universal amplitude $A_{q=2}^{C,I}$ is plotted as function of s . Notice that in the limit of small s (the limit in which the torus reduces to a cylinder) $A_{q=2}^{C,I}$ approaches the value of $\pi/4$, in accordance with Eq. (3.15).

Our exact expressions for the finite-size-scaling behavior, Eqs. (5.6) and (5.8) agree with the results of the Onsager solution of the Ising model. Ferdinand and Fisher¹⁴ [see Eq. (3.37) in their paper], found the following expressions for the scaling parts of the four partition functions:

$$\begin{aligned} Z_{q=2}^P &\propto \frac{1}{2\eta} [\theta_2(s) + \theta_3(s) + \theta_4(s)], \\ Z_{q=2}^{I,C} &\propto \frac{1}{2\eta} [\theta_2(s) + \theta_3(s) - \theta_4(s)], \\ Z_{q=2}^{C,I} &\propto \frac{1}{2\eta} [-\theta_2(s) + \theta_3(s) + \theta_4(s)], \\ Z_{q=2}^{C,C} &\propto \frac{1}{2\eta} [\theta_2(s) - \theta_3(s) + \theta_4(s)], \end{aligned} \quad (5.9)$$

where θ_2 and θ_4 are different types of Jacobi's θ functions, defined as

$$\begin{aligned} \theta_4(z) &= \sum_{n \in \mathbb{Z}} (-1)^n \exp(-\pi z n^2), \\ \theta_2(z) &= \frac{1}{\sqrt{z}} \theta_4 \left[\frac{1}{z} \right]. \end{aligned} \quad (5.10)$$

We checked numerically that the coefficients of the expansion in powers of $\exp(-\pi/12s)$ in Eqs. (5.6) and (5.8) are identical to those in Eqs. (5.9). We leave it to an interested reader to find an analytical proof of the equivalence.

Consider the three-state Potts model ($q=3$). From Eqs. (3.4) and (3.11) it follows that $y = \frac{1}{3}$ and $K_g = \pi x = \frac{5}{3}\pi$. At this value of q there are three different types of G operators: I , C , and T (see Table I). It is straightforward to evaluate the finite-size-scaling parts of the partition functions of the six commuting pairs G, \tilde{G} in the same manner as in Eq. (5.6). The results are listed in Table III. Similar to the Ising case, the following relation holds $Z_{q=3}^P = Z_{q=3}^{I,C} + Z_{q=3}^{C,I} + Z_{q=3}^{C,C} + Z_{q=3}^{C,C^{-1}}$. In Fig. 1 the universal amplitude $A_{q=3}^{C,I}$ is plotted as function of s .

Finally consider the four-state Potts model ($q=4$). From Eqs. (3.4) and (3.11) it follows that $y=0$ and $K_g = \pi x = 2\pi$. Now there are five different types of G operators: I , C , T_0 , T_1 , and T_2 (see Table I). The partition functions of the 15 commuting pairs G, \tilde{G} , and the corresponding universal amplitudes are listed in Table IV. Notice that

$$Z_{q=4}^P = Z_{q=4}^{I,T_0} + Z_{q=4}^{T_0,I} + Z_{q=4}^{T_0,T_0} + Z_{q=4}^{T_0,T_0'} + Z_{q=4}^{T_0',T_0}.$$

$A_{q=4}^{C,I}$ is plotted in Fig. 1.

In the limit of zero aspect ratio, $s \rightarrow 0$, Eq. (4.9) reduces to Eq. (3.13) for the cylinder. In this limit only the $P_2=0$ sector contributes in Eq. (4.9). $Z_g^{P_1, P_2}$ vanishes unless $P_2=0$, see Eq. (4.10). This means that only nonhomotopic polygons of type (1,0) contribute. These are indeed the only types of nonhomotopic polygons that are allowed on a cylinder. The weight \sqrt{C} of these polygons is simply equal to $C(G, \tilde{G}; 1, 0) = n_1$. In the limit of small s the summation over P_1 in Eq. (4.9) can be converted into a Gaussian integral,

$$\begin{aligned} Z_q^{G\tilde{G}} &\approx Z_g^{0,0} \int_{-\infty}^{\infty} dP_1 \exp \left[-\frac{\pi x}{2} s P_1^2 \right] \left\{ \exp(i\pi \alpha P_1) + \frac{1}{2} [T(G, \tilde{G}) - 1] \exp(i\pi P_1) \right\} \\ &\approx \exp \left[\frac{\pi}{6s} \right] \left[\exp \left[-\frac{\pi \alpha^2}{2sx} \right] + \frac{1}{2} [T(G, \tilde{G}) - 1] \exp \left[-\frac{\pi}{2sx} \right] \right]. \end{aligned} \quad (5.11)$$

The factor outside the bracket originates from the small s expansion of the eta function in $Z_g^{0,0}$ [see Eq. (4.11)]. As expected we recover Eqs. (3.13) and (3.16). The second term in the above equation (torus-cluster contributions)

can be neglected. Notice that $|\alpha| \leq 1$ [see Eq. (4.6)]. At $\alpha=1$ the torus-cluster contributions come into play but only change the overall factor from unity to $\frac{1}{2}[T(G, \tilde{G}) + 1]$.

TABLE II. Finite-size-scaling contributions of the partition functions, $Z_{q=2}^{G\tilde{G}}$, of the Ising model on a torus. See Eqs. (5.2)–(5.4) for the definition of $[n, m]$. The values of the universal finite-size-scaling amplitudes, $A_{q=2}^{G\tilde{G}}(s)$, are listed for the aspect ratios $s = 1, \frac{1}{2}\sqrt{3}$, and $\frac{1}{2}$.

G	\tilde{G}	$Z_{q=2}^{G\tilde{G}}$	$A_{q=2}^{G\tilde{G}}(1)$	$A_{q=2}^{G\tilde{G}}(\frac{1}{2}\sqrt{3})$	$A_{q=2}^{G\tilde{G}}(\frac{1}{2})$
I	I	$4[4, 4] - [1, 1]$			
C	I	$4[4, 4] - [1, 1] + 2[2, 1] - 4[4, 2]$	0.9865	0.9716	0.8709
C	C	$-4[4, 4] + [1, 1] - 2[2, 1] + 4[4, 2]$ $- 2[1, 2] + 4[2, 4]$	1.3695	1.2009	0.8889

TABLE III. Finite-size-scaling contributions of the partition functions, $Z_{q=3}^{G\tilde{G}}$ of the three-state Potts model on a torus. See Eqs. (5.2)–(5.4) for the definition of $[n, m]$. The values of the universal finite-size-scaling amplitudes, $A_{q=3}^{G\tilde{G}}(s)$, are listed for the aspect ratios $s = 1, \frac{1}{2}\sqrt{3}$, and $\frac{1}{2}$.

G	\tilde{G}	$Z_{q=3}^{G\tilde{G}}$	$A_{q=3}^{G\tilde{G}}(1)$	$A_{q=3}^{G\tilde{G}}(\frac{1}{2}\sqrt{3})$	$A_{q=3}^{G\tilde{G}}(\frac{1}{2})$
I	I	$6[6, 6] - 3[3, 3] + 2[2, 2] - [1, 1]$			
C	I	$6[6, 6] - 3[3, 3] + 2[2, 2] - [1, 1]$ $+ 3[3, 1] - 6[6, 2]$	1.1874	1.1560	0.9807
C	$C(C^{-1})$	$-3[6, 6] + \frac{3}{2}[3, 3] - [2, 2] + \frac{1}{2}[1, 1]$ $-\frac{3}{2}[3, 1] + 3[6, 2] - \frac{3}{2}[1, 3] + 3[2, 6]$	1.6348	1.4290	1.0051
T	I	$6[6, 6] + 3[3, 3] - 2[2, 2] - [1, 1]$ $+ 2[2, 1] - 6[6, 3]$	0.6224	0.5854	0.4325
T	T	$-6[6, 6] - 3[3, 3] + 2[2, 2] + [1, 1]$ $- 2[2, 1] + 6[6, 3] - 2[1, 2] + 6[3, 6]$	0.7571	0.6600	0.4360

TABLE IV. Finite-size-scaling contributions of the partition functions, $Z_{q=4}^{G\tilde{G}}$ of the four-state Potts model on a torus. See Eqs. (5.2)–(5.4) for the definition of $[n, m]$. The values of the universal finite-size-scaling amplitudes, $A_{q=4}^{G\tilde{G}}(s)$, are listed for the aspect ratios $s = 1, \frac{1}{2}\sqrt{3}$, and $\frac{1}{2}$.

G	\tilde{G}	$Z_{q=4}^{G\tilde{G}}$	$A_{q=4}^{G\tilde{G}}(1)$	$A_{q=4}^{G\tilde{G}}(\frac{1}{2}\sqrt{3})$	$A_{q=4}^{G\tilde{G}}(\frac{1}{2})$
I	I	$6[2, 2] - [1, 1]$			
C	I	$2[2, 2] - [1, 1] + 4[4, 1] - 4[4, 2]$	1.4197	1.3421	1.0202
C	$C(C^{-1})$	$4[2, 2] + [1, 1] - 2[2, 1] - 2[1, 2]$	1.7535	1.5295	1.0302
T_0	I	$-2[2, 2] - [1, 1] + 4[2, 1]$	1.4197	1.3421	1.0201
T_0	T_0	$6[2, 2] + 3[1, 1] - 4[2, 1] - 4[1, 2]$	1.7357	1.5149	1.0275
T_1	I	$-[1, 1] + 3[3, 1]$	0.8409	0.7738	0.5320
T_1	$T_1(T_1^{-1})$	$\frac{9}{2}[3, 3] + \frac{1}{2}[1, 1] - \frac{3}{2}[3, 1] - \frac{3}{2}[1, 3]$	0.9679	0.8420	0.5348
T_2	I	$-2[2, 2] - [1, 1] + 2[2, 1] + 4[4, 2]$	0.4766	0.4336	0.2884
T_2	T_2	$8[4, 4] + 6[2, 2] + [1, 1]$ $- 2[2, 1] - 4[4, 2] - 2[1, 2] - 4[2, 4]$	0.5308	0.4615	0.2892
$T_0(1, 2; 3, 4)$	$T_0'(1, 3; 2, 4)$	$2[2, 2] - [1, 1]$	1.7716	1.5444	1.0328
$T_2(1; 2; 3, 4)$	$T_2'(3; 4; 1, 2)$	$8[4, 4] - 2[2, 2] - [1, 1]$ $+ 2[2, 1] - 4[4, 2] + 2[1, 2] - 4[2, 4]$	1.4197	1.2183	0.5921
$T_2(1; 2; 3, 4)$	$T_0(1, 2; 3, 4)$	$-2[2, 2] + [1, 1] - 2[2, 1] + 4[4, 2]$	1.5653	1.2890	0.5937
$C(1, 3, 2, 4)$	$T_0(1, 2; 3, 4)$	$-2[2, 2] - [1, 1]$ $+ 4[2, 1] - 4[4, 1] + 4[4, 2]$	1.7716	1.5444	1.0328

ACKNOWLEDGMENTS

This work is supported by National Science Foundation Grant No. DMR-85-09392 and one of us (M.dN.) was supported in part by the Alfred Sloan Foundation.

APPENDIX: TOPOLOGICAL PROPERTIES OF CLUSTERS, LAKES, AND POLYGONS ON A TORUS

In this appendix we summarize several topological aspects of clusters, lakes, and polygons on a torus, and also our notation and sign conventions. More details can be found in textbooks on topology.²¹

(1) In this paper contours and polygons are non-self-intersecting closed loops on the torus, while loops and walks are allowed to be self-intersecting. The word polygon is used as a synonym for a coastline between a cluster and a lake.

(2) Polygons and contours on the torus are characterized by their winding numbers, (ω_1, ω_2) . Figure 7 shows a (1,2) contour, and Fig. 8 shows a (2,5) contour. (0,0) type contours on the torus are homotopic; they can be contracted to a point. Contours with nonzero winding numbers are nonhomotopic.

(3) To each torus we associate two seams. When you cut the torus along these seams, you obtain a plane with equal opposite sides (L_1, L_2) . Assume that $L_1 \leq L_2$. The meridian seam is a (0,1) type contour, and the longitudinal seam a (1,0) type contour. The shape and location of the seam are arbitrary. The seams are fully characterized

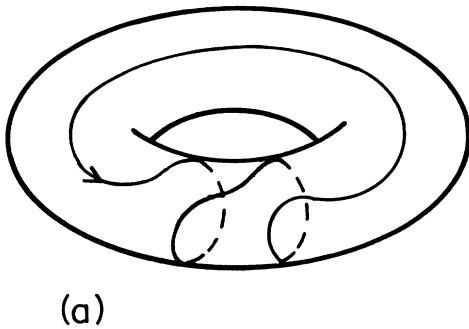
by their winding numbers and by an arrow on top of them (see Fig. 2). The arrow gives the seams a directional sense, and is used to prescribe the relative signs of the winding numbers of contours: a $\omega_1 (\omega_2)$ contour wraps around the torus $\omega_1 (\omega_2)$ times in the direction of the arrow on the longitudinal (meridian) seam (see Figs. 7 and 8).

(4) The winding numbers ω_1 and ω_2 of contours and polygons are coprime (they have no common divisor except 1). Imagine that you tile the plane with Fig. 7(b) or 8(b) as unit cell. This creates a pattern of periodic nonintersecting lines across the plane. If ω_1 and ω_2 are coprime, then all these lines are shifted copies of each other. The pattern along the line is also periodic. It repeats itself after $\omega_1 \times \omega_2$ unit cells. If ω_1 and ω_2 have a common divisor, say n , then the structure along the line repeats itself after $\omega_1 \times \omega_2 / n$ unit cells, and instead of one there are n different types of lines in the pattern. In other words, a unit cell like Fig. 7(b) represents n independent contours if ω_1 and ω_2 are not coprime.

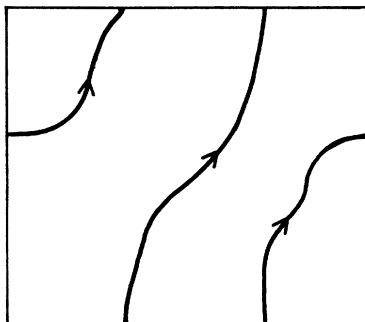
(5) In a configuration with several contours, the winding numbers (ω_1, ω_2) of all the contours with nonzero winding numbers must be the same.

(6) Clusters and lakes on the torus are also characterized by a set of winding numbers. Consider all possible closed contours across the cluster. The set of possible winding numbers of these contours characterizes the cluster (lake).

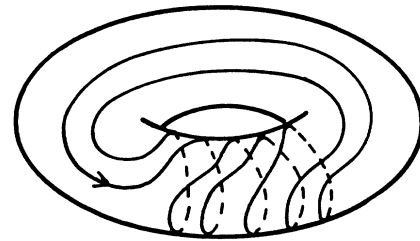
(7) An island (pond) is a cluster (lake) on which only



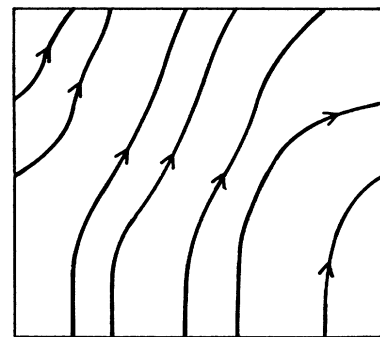
(a)



(b)



(a)



(b)

FIG. 7. A nonhomotopic contour with winding numbers (1,2).

FIG. 8. A nonhomotopic contour with winding numbers (2,5).

(0,0) contours are possible [see Figs. 6(a) and 6(c)]. Notice that a (0,0) type contour around a pond inside a cluster is nonhomotopic. It cannot be contracted to a point, because it cannot intersect the coastline between the cluster and the pond.

(8) A cylinder cluster (lake) is a cluster (lake) on which only one type of contour with nonzero winding numbers is possible. Figure 6(b) shows a (1,2) cylinder cluster. Besides (0,0) contours only contours with winding numbers (1,2) are possible. We refer to these clusters as cylinder clusters (and cylinder lakes) because they have the topology of a cylinder (although they are embedded on a torus).

(9) The winding numbers ω_1 and ω_2 of cylinder clusters and cylinder lakes are coprime.

(10) In a configuration with several cylinder clusters and cylinder lakes, the winding numbers of all the cylinder clusters and all the cylinder lakes are the same.

(11) The number of cylinder clusters in a configuration is equal to the number of cylinder lakes. For example, the construction of the (1,2) cylinder cluster in Fig. 6(b) creates automatically a (1,2) cylinder lake.

(12) A torus cluster (torus lake) is a cluster (lake) on which two independent types of contours with nonzero winding numbers are possible. Figure 9(a) shows the simplest torus cluster shape. Clearly both (0,1) and (1,0) contours are possible. Torus clusters and torus lakes have the same topology as the torus on which they are embedded.

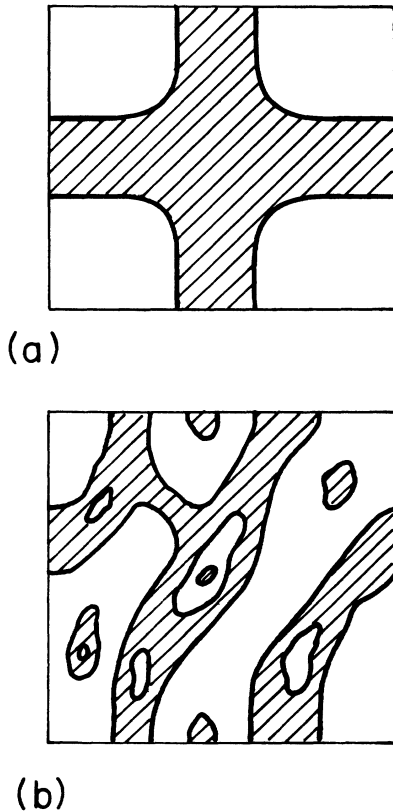


FIG. 9. Torus clusters on a torus. (a) The simplest torus-cluster shape, (b) a torus cluster obtained by adding a bridge to a (1,2) cylinder cluster.

(13) A configuration can contain only one torus cluster or one torus lake.

(14) In a configuration where all lakes (clusters) are ponds (islands) there exist one and only one torus cluster (torus lake) and no cylinder clusters or cylinder lakes.

(15) In a configuration with cylinder clusters and cylinder lakes, torus clusters, and torus lakes are absent.

(16) On every torus cluster and torus lake it is possible to draw a (0,1) and a (1,0) type contour. For example, Fig. 9(b) shows a torus cluster obtained by adding a bridge to a (1,2) cylinder cluster. This cluster is topologically equivalent to the cluster in Fig. 9(a). We can unwind it by reshaping the coastline without merging, splitting, or intersecting the coastline with itself. The addition of the bridge transforms the (1,2) cylinder lake into a pond. Imagine that you tile the plane with Fig. 9(b) as unit cell. That leads to a percolating connected cluster in both the vertical and horizontal directions (all the lakes are ponds). Therefore it is possible to walk all the way across the cluster from the left to the right and from the top to the bottom. These walks represent the (0,1) and (1,0) contours. Projected back into the unit cell Fig. 9(b), or shown on the torus, these contours tend to look quite complex.

(17) Consider the set of all configurations with n cylinder clusters. This set is self-dual, i.e., maps into itself when we exchange lakes and clusters. The clusters and lakes in the Potts model have a lattice structure (Fig. 4) instead of being continuum-type objects (Fig. 6). Then this duality requires also a translation over a lattice vector \mathbf{a} of the surrounding lattice \mathcal{S} (see Fig. 4) and requires that lattice \mathcal{L} is self-dual.

(18) Consider the set of all configurations with one torus cluster, and also the set of all configurations with one torus lake. These sets map into each other under the same type of duality as in (17), i.e., under exchange of lakes and clusters.

(19) On every graph, i.e., lattice-type configuration with clusters and lakes (see Fig. 4), the Euler relation states that the number of clusters N_c , the number of sites N_s , the number of bonds N_b , and the number of independent nonhomotopic contours on the clusters N_l , are related as $N_c = N_s - N_b + N_l$.

(20) The number of homotopic coastlines in a configuration is equal to the number of ponds plus the number of islands. The number of nonhomotopic coastlines, N_{nhp} is twice the number of cylinder clusters, $N_{\text{nhp}} = 2N_{\text{nhc}}$. Also notice that a torus cluster configuration without any pond or island does not contain any coastline. So the total number of coastlines in any configuration, N_p , is equal to the number of ponds plus the number of islands plus twice the number of cylinder clusters.

(21) In configurations with one torus lake [all clusters are islands, see Fig. 6(a)] the number of independent nonhomotopic contours on the clusters, N_l , is equal to the number of ponds (you can walk around every pond, but not around the torus lake). Therefore, the number of coastlines, N_p , is equal to $N_p = N_c + N_l$. Every coastline is a (0,0) type contour.

(22) In configurations with one torus cluster [all lakes

are ponds, see Fig. 6(c)] N_l is equal to the number of ponds minus 1 (you can walk around every pond but the contour which encompasses all ponds is homotopic) plus 2 [you can circumnavigate the torus via a (0,1) or (1,0) contour on the torus cluster]. Notice that on a lattice there is always at least one pond. Therefore, [see (20)] the number of coastlines, N_p , is equal to $N_p = N_c + N_l - 2$. Every coastline is a (0,0) type contour.

(23) In configurations with cylinder clusters and cylinder lakes [Fig. 6(b)] N_l is equal to the number of ponds plus the number of cylinder clusters [you can walk around every pond or circumnavigate the torus via a (ω_1, ω_2) contour on each cylinder cluster]. The total number of coastlines in the configuration, N_p is equal to $N_p = N_c + N_l$.

*Address after September 1, 1988: Department of Physics, Carnegie-Mellon University, Pittsburgh, PA 15213.

¹M. den Nijs, *J. Phys. A* **12**, 1857 (1979); *Phys. Rev. B* **27**, 1674 (1983); *J. Phys. A* **17**, L295 (1984).

²B. Nienhuis, in *Phase Transitions and Critical Phenomena*, edited by C. Domb and J. L. Lebowitz (Academic, London, 1987), Vol. 11.

³J. L. Cardy, in *Phase Transitions and Critical Phenomena*, edited by C. Domb and J. L. Lebowitz (Academic, London, 1987), Vol. 11.

⁴J. L. Cardy, *Nucl. Phys. B* **270** [FS16], 186 (1986); **275** [FS17], 200 (1986).

⁵H. W. J. Blöte, J. L. Cardy, and M. P. Nightingale, *Phys. Rev. Lett.* **56**, 742 (1986).

⁶I. Affleck, *Phys. Rev. Lett.* **56**, 746 (1986).

⁷H. Park and M. den Nijs (unpublished).

⁸M. Barber, in *Phase Transitions and Critical Phenomena*, edited by C. Domb and J. L. Lebowitz (Academic, London, 1983), Vol. 8; M. P. Nightingale, *J. Appl. Phys.* **53**, 7927 (1982).

⁹H. W. J. Blöte and M. den Nijs, *Phys. Rev. B* **37**, 1766 (1988).

¹⁰M. den Nijs, in *Phase Transitions and Critical Phenomena*, edited by C. Domb and J. L. Lebowitz (Academic, London, 1988), Vol. 12.

¹¹R. J. Baxter, S. B. Kelland, and F. Y. Wu, *J. Phys. A* **9**, 397 (1976).

¹²H. J. F. Knops, *Ann. Phys. (N.Y.)* **128**, 448 (1980).

¹³P. di Francesco, H. Saleur, and J. B. Zuber, *J. Stat. Phys.* **49**, 57 (1987).

¹⁴A. E. Ferdinand and M. E. Fisher, *Phys. Rev.* **185**, 832 (1969).

¹⁵C. M. Fortuin and P. W. Kasteleyn, *Physica* **57**, 536 (1972).

¹⁶E. H. Lieb, *Phys. Rev. Lett.* **18**, 1046 (1967).

¹⁷H. van Beijeren, *Phys. Rev. Lett.* **38**, 993 (1977).

¹⁸R. J. Baxter, *Exactly Solved Models in Statistical Mechanics* (Academic, London, 1982).

¹⁹C. B. Thorn, *Phys. Rep.* **67**, 171 (1980).

²⁰Bateman Manuscript Project, *Higher Transcendental Functions* (McGraw-Hill, New York, 1953), Vol. 2.

²¹D. Rolfsen, *Knots and Links* (Publish or Perish, Berkeley, 1976).

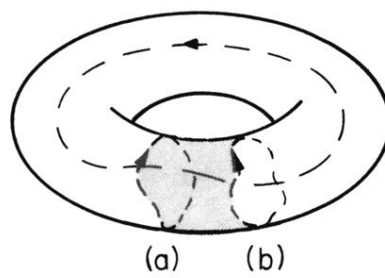


FIG. 3. Gauge invariance of seams on a torus.